

One-Dimensional Microfluidic Crystals Far from Equilibrium

— *Acoustic Phonons, Instabilities and Confinement* —

Tsevi BEATUS,¹ Roy BAR-ZIV¹ and Tsvi TLUSTY²

¹*Department of Materials and Interfaces,
The Weizmann Institute of Science, Rehovot, Israel*

²*Physics of Complex Systems,
The Weizmann Institute of Science, Rehovot, Israel*

We investigated the collective motion of a one-dimensional array of water-in-oil droplets flowing in microfluidic channel in quasi-2D at low Reynolds number. Driven far from equilibrium by the symmetry-breaking flow field, the droplets exhibit acoustic normal modes (crystal ‘phonons’) with unusual dispersion relations. These phonons are due to long-range hydrodynamic dipolar interactions between the droplets. The phonon spectra change anomalously at the crossover between unconfined 2D flow and 1D confined flow, as a result from an interplay between boundary-induced screening and crystal incompressibility. Microfluidic crystals offer a vista, in the linear flow regime, into soft-matter systems far from equilibrium.

§1. Introduction

The understanding of non-equilibrium dynamics lags well behind the advanced theory of systems at thermal equilibrium. A system at equilibrium can be described by a free-energy functional, whose minimization predicts the system’s behavior. Beyond equilibrium, however, this approach breaks down – energy functionals cannot be defined, which renders the formulation of a general non-equilibrium theory a difficult problem. Microfluidic two-phase flow offers experimental tools to investigate dissipative non-equilibrium dynamics.^{1)–10)} Among the simplest systems in this class are microfluidic crystals – ordered one-dimensional (1D) arrays of water-in-oil droplets driven by flow.^{11),12)} Microfluidic crystals are of particular interest since they are governed by long-range interactions and operate in the linear flow regime. These interactions share common features with other systems driven by a symmetry-breaking field, such as dusty-plasma crystals,^{13),14)} vortices in superconductors,^{15),16)} non-Brownian sedimentation,¹⁷⁾ ordered arrays of micro-spheres,¹⁸⁾ active membranes¹⁹⁾ and nucleoprotein filaments.^{20),21)} Thus, microfluidic crystals offer insight, in the linear flow regime, into many-body physics far from equilibrium.

We started by studying 1D microfluidic crystals of disc-like droplets flowing in a 2D channel. The Reynolds number of this system is very low, around 10^{-4} , hence vibrations due to inertia are over-damped. Surprisingly, we found that the crystal carries phonon-like vibrational modes that propagate at sound velocity of $\sim 100 \mu\text{ms}^{-1}$ and frequencies of $\sim 1\text{Hz}$. Importantly, these fluctuations are not thermal, since they are unobservable without flow. These phonons exhibit unusual dispersion markedly different than those of harmonic crystals and give rise to a variety of non-linear crystal instabilities. We developed a first-principles theory showing that these phonons result from the symmetry-breaking flow field, which induces long-range inter-droplet

hydrodynamic interactions.¹¹⁾ Next, we investigated how the phonon spectra change at the crossover between a 2D flow and a confined 1D flow,¹²⁾ and found that confinement has a dramatic effect on these spectra. The sidewall boundaries induce weakening and screening of the interactions, but when approaching the 1D limit, we measured a marked increase in the crystal sound velocity — a sign of interaction strengthening. This non-monotonous behavior of the phonon spectra was explained theoretically by the interplay of screening and incompressibility.

§2. Experimental setup

The microfluidic device (Fig. 1) was fabricated using standard soft-lithography and made of poly-dimethyl-siloxane (PDMS).^{1),11)} Water droplets formed at a T-junction between water and oil channels under continuous flow, emanating at constant rate with uniform radii $R \sim 10 - 40 \mu\text{m}$. The T-junction, $20 - 30 \mu\text{m}$ in width, was connected to a wider channel of width W , where the droplets formed an ordered 1D array with uniform spacing $a \sim 10 - 200 \mu\text{m}$. The height h of the channel was $10 \mu\text{m}$ and since $h < 2R$, the droplets had a disc-like shape, squeezed between the channel floor and ceiling. These boundaries induced a frictional force, rendering the droplets velocity $u_d \sim 150 - 500 \mu\text{ms}^{-1}$ slower than the velocity of the dragging oil, $u_{oil} \sim 5u_d$.¹¹⁾ The crystal and flow parameters were controlled by adjusting the pressures at the water and oil inlets. Using a motorized microscope stage we followed the droplets, moving in their mean velocity u_d , and recorded their images using a CCD camera, such that in a typical experiment we followed up to 60 droplets for ~ 40 s. The droplet trajectories were extracted from the images using Matlab.^{11),12)}

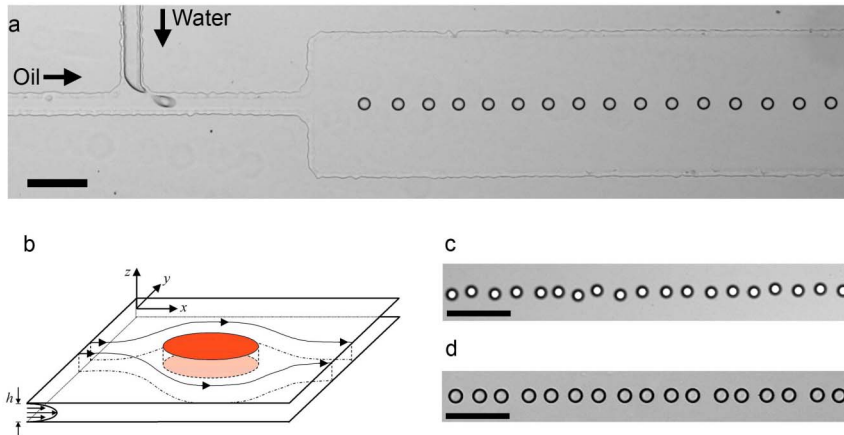


Fig. 1. (a) Droplets of water-in-oil (mineral oil, viscosity 30 mPa·s, with 2% span-80 surfactant (w/w)) were formed at a T-junction under constant pressure. (b) Channel height was $10 \mu\text{m}$, smaller than the droplet radii R , thus deforming them into discs. (c, d) Images of transversal (c) and longitudinal (d) acoustic waves.

§3. Phonons and instabilities in unconfined crystals

Following the moving crystal in its frame of reference, we tracked the positions of droplets in time and subsequently applied a Fourier transform in space and time to these data. Thus, we obtained the power-spectra of both the longitudinal and transversal vibrations in terms of wave-number k and frequency ω (Figs. 2(a) and (b)). The peaks of the power-spectrum define the dispersion relation of modes $\omega(k)$. The main feature of the dispersion in a sine-like curve with the following properties: (a) Around $k = 0$ we have $\omega(k) = C_s k$, which corresponds to acoustic waves with a sound velocity $C_s \sim 250 \mu\text{ms}^{-1}$. (b) Close to the edges of Brillouin zone at $k = \pm\pi/a$ the acoustic waves travel oppositely at $-C_s/2$. (c) The longitudinal and transversal dispersion relations are identical in magnitude and form but are anti-symmetric, $\omega_x(k) = -\omega_y(k)$. (d) Standing waves appear at the middle of Brillouin zone and not at its edges. The standing waves are the modes with highest frequency in the system $\sim 1\text{Hz}$. A secondary feature is a straight line $\omega(k) = -u_d k$, which stems from stationary defects that in the frame of the moving crystal seem to be moving backwards. These defects deflect the droplets, creating waves that travel at velocity $-u_d$ for all k values. Hence, this trivial linear dispersion is not related to the hydrodynamic interactions between the droplets. The sine-like curve corresponds to the collective normal modes of the crystal, which are similar to solid-state

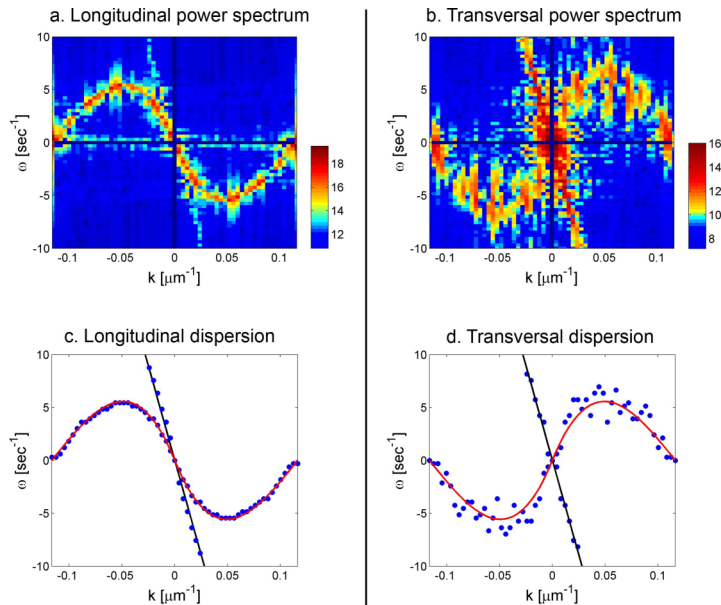


Fig. 2. (color online) Intensity plots of the logarithm of power-spectrum of longitudinal (a) and transversal (b) waves as a function of wave-vector and frequency (k, ω) . The corresponding dispersion relations (c, d) are the peaks of the power spectrum. The skewed sine-like curve is due to the hydrodynamic interactions. The red line in the theoretical calculation for $\omega(k)$ with no adjustable parameters. The black straight line $\omega(k) = -u_d k$ is due to droplet deflections by stationary defects along the channel.

‘phonons’. As we now explain theoretically, the unusual dispersion of these phonons arises from hydrodynamic interactions between the droplets, that are induced by the symmetry breaking flow field.

The flow perturbation induced by the disc-like droplet is well approximated by a potential flow in 2D, such that the velocity of the perturbation is the gradient of the potential ϕ_d , which satisfies the Laplace equation:¹¹⁾

$$\phi_d(\mathbf{r}) = R^2(u_{oil}^\infty - u_d) \frac{\mathbf{r} \cdot \hat{\mathbf{x}}}{r^2}, \quad (3.1)$$

where u_{oil}^∞ is the oil velocity far from the droplet and \mathbf{r} is the displacement from the center of the droplet. Droplets i and j interact with each other via the drag force, directed along the dipole velocity field $F_{drag} = \xi_d \nabla \phi_d(\mathbf{r}_i - \mathbf{r}_j)$ with a drag coefficient $\xi_d = 8\pi\eta R^2/h$ (η is oil viscosity). The dipolar interaction is illustrated in Fig. 3(a). The potential of the whole crystal is approximately a superposition of single-droplet potentials $\phi(\mathbf{r}) = u_{oil}^\infty \mathbf{r} \cdot \hat{\mathbf{x}} + \sum_j \phi_d(\mathbf{r} - \mathbf{r}_j)$. Besides the drag force, the droplets are subject to a force of friction with the channel floor and ceiling, $F_{fric} = \mu u_d$, where μ is a friction coefficient. Without inertia, drag and friction must balance out $\mu u_d = \xi_d(u_{oil}(\mathbf{r}) - u_d)$. Solving for u_d gives the droplet’s equation of motion $\dot{\mathbf{r}} = (u_d^\infty/u_{oil}^\infty) \sum_{j \neq n} \nabla \phi_d(\mathbf{r}_n - \mathbf{r}_j)$.¹¹⁾ Expanding in small deviations from the crystal positions $(x_n, y_n) \ll a$ leads to wave equations, with the dispersion relations:

$$\omega_x(k) = \frac{6C_s}{\pi^2 a} \sum_{j=1}^{\infty} \frac{\sin(jka)}{j^3} \quad ; \quad \omega_y(k) = -\omega_x(k), \quad (3.2)$$

$$C_s = \frac{2\pi^2}{3} \left(\frac{R^2}{a^2} \right) \left(\frac{u_d^\infty}{u_{oil}^\infty} \right) (u_{oil}^\infty - u_d^\infty). \quad (3.3)$$

This theoretical result fits the data without any adjustable parameters (Figs. 2(c) and (d)). The sound velocity scale C_s reflects a convergent summation over long range forces along the crystal that are induced by the symmetry-breaking field.

Interestingly, even without perturbations, the velocity of the droplets depends on the crystal spacing a , since the longitudinal force acting on every droplet is directed against the flow. Crystal velocity, therefore, decreases with a (Fig. 3(b)), which explains the existence of long-wavelength longitudinal density waves.

The crystal undergoes instabilities leading to breakup and disorder. These occur upon large-amplitude fluctuations, either at the middle of the crystal or close to the droplet formation area (Fig. 4). The instabilities can only be understood when considering the non-linear nature of the dipolar interaction.¹¹⁾

§4. The anomalous effect of boundaries on the phonons

So far we discussed unconfined microfluidic crystals, in which the channel side-walls are very far from the droplets (Fig. 1(a)). Next, we investigated the crystal under different degrees of confinement (Fig. 5(a)), ranging from unconfined flow in 2D to 1D flow, where the channel is nearly blocked by the droplets (‘plug-flow’).¹²⁾

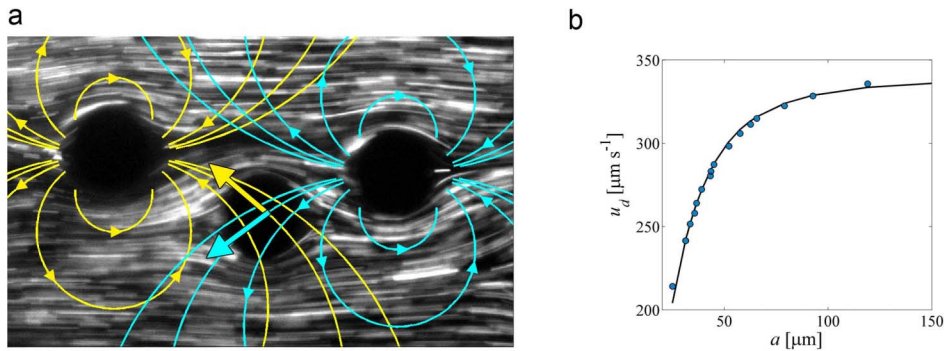


Fig. 3. (color online) (a) Stream lines of oil flow imaged with fluorescent beads. The flow is from left to right. Superimposed are the dipole fields $\nabla\phi_a$ of two droplets applying a drag force on the middle droplet (bold arrows). The longitudinal components of both forces are directed against the flow and do not cancel out. (b) Velocity of droplets as a function of crystal spacing: data (blue circles) and theory (solid line). Here, $u_{oil} \sim 1900 \mu\text{ms}^{-1}$ and $R \sim 10 \mu\text{m}$.

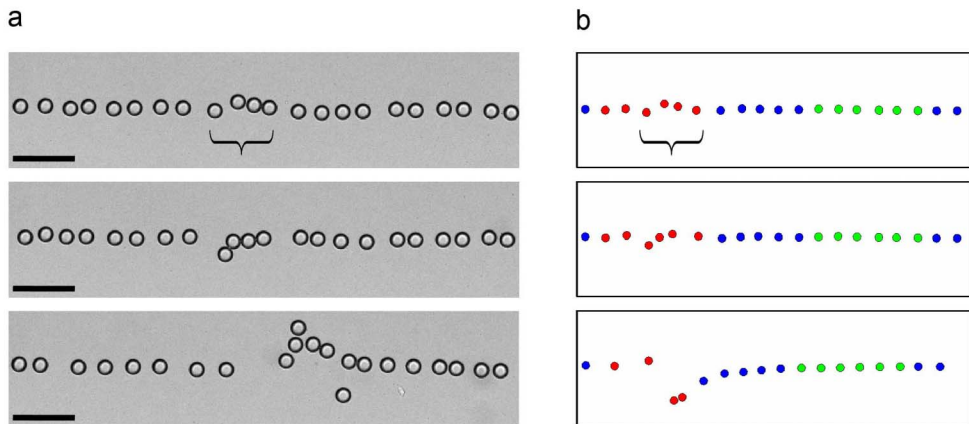


Fig. 4. (a) Subsequent images taken $0.3s$ apart, of a local fluctuation (four droplets, marked) that grows and leads to crystal instability. Flow direction is from left to right. All scale-bars are $100 \mu\text{m}$. (b) Similar dynamics is obtained by simulating the non-linearized equations of motion.

We measured the phonon spectra upon narrowing the channel width, varying the confinement parameter, $\gamma \equiv 2R/W$, from 0.1 ($W = 250 \mu\text{m}$, practically unconfined) to 0.9 ($W = 50 \mu\text{m}$). Under confinement, the general shape of the spectra remained. However, the longitudinal-transversal anti-symmetry was broken: $|\omega_x(k)| < |\omega_y(k)|$ for all $k < \pi/a$ (Fig. 5(b)). This is evident in Fig. 5(c), showing the sound velocities $C_{s,x}$ and $C_{s,y}$, normalized by the theoretically computed unconfined $C_s(\gamma = 0)$ (Eq. (3)).¹¹ For the longitudinal phonons, $C_{s,x}$ decreased as γ increased. Above $\gamma \sim 0.6$ the sine-like curve fell below our detection limit. Oppositely, for the transversal phonons $C_{s,y}$ increased with γ . However, the amplitude of phonons decreased exponentially with γ (Fig. 5(d)), essentially undetectable above $\gamma \sim 0.65$. To con-

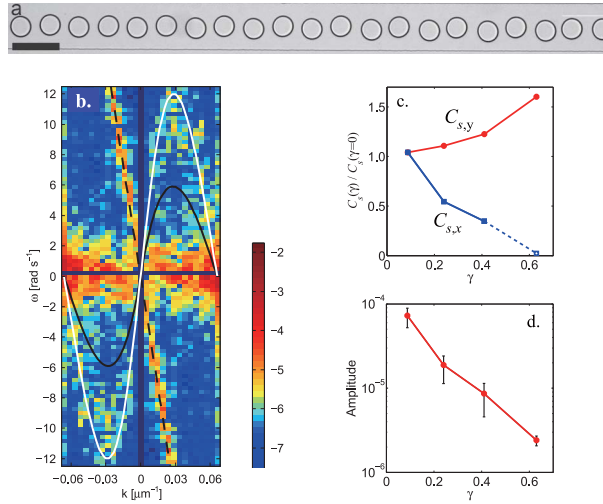


Fig. 5. (a) The microfluidic crystal under confinement of $\gamma = 0.46$ in a channel of width $W = 100 \mu\text{m}$. The phonons are easily observed. Scale-bar is $100 \mu\text{m}$. (b) The power-spectrum of transversal modes for confinement of $\gamma = 0.63$, $W = 70 \mu\text{m}$, $u_{oil} = 1500 \mu\text{ms}^{-1}$, $u_d = 490 \mu\text{ms}^{-1}$. The resulting $C_{s,y}$ was $700 \mu\text{ms}^{-1}$. (c) $C_s(\gamma)/C_s(\gamma=0)$ for both polarizations. $C_s(\gamma=0)$ was calculated from theory for an unconfined crystal with the same flow parameters as the confined one. (d) Mean amplitude of the transversal modes as a function of γ .

clude, under confinement we observed that C_s decreased in the longitudinal modes but increased in the transversal ones. Additionally, the amplitude of vibrations of both modes decreased significantly.¹²⁾

The hydrodynamic potential of a droplet under confinement can be calculated using the method of image charges, used in electrostatics, to account for the zero mass-flux through the sidewall boundaries. We introduce an array of image dipoles perpendicular to the flow.²²⁾ When the droplet is in the middle of the channel ($y = 0$, Fig. 6(a)), this array of images has a lattice constant of W . If the droplet deviates from the middle ($y = \delta \neq 0$, Fig. 6(b)), its images array splits into two interlaced arrays of lattice constant $2W$, displaced with respect to each other by 2δ . The difference between $\delta = 0$ and $\delta \neq 0$ is the source of the $x - y$ anti-symmetry breaking.¹²⁾

The image array provides intuition for how the sidewalls screen the long-range dipolar interactions. Far from the droplet, the image dipoles can be considered as a parallel plate capacitor, hence, the electrostatic field outside the capacitor vanishes. However, since the array is discrete and not continuous, the field leaks out, and decays exponentially as $\exp(-2\pi r/W)$.^{12), 23)}

The single-droplet confined potential can be calculated by summing the contributions of the droplet and its images.¹²⁾ The asymptotic spatial dependence of the single-droplet velocity field is, therefore:

$$\partial_x \phi \sim (u_{oil}^\infty - u_d) \begin{cases} \gamma \tan(\pi\gamma/2) \exp(-2\pi x/W), & x \gg W \\ R^2/x^2, & x \ll W. \end{cases} \quad (4.1)$$

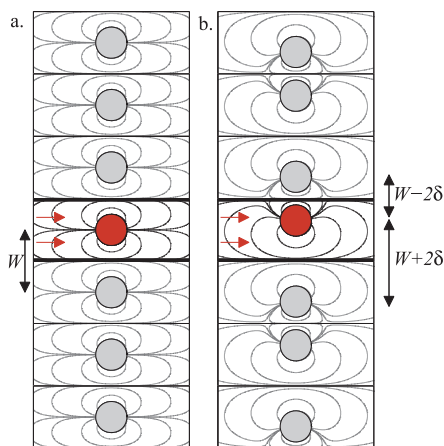


Fig. 6. (color online) Flow lines around a single confined droplet (dark blue) are the result of summing the dipole flow fields of its infinite array of reflections (gray). (a) When the droplet is at the center of the channel, the array has uniform spacing W . (b) When the droplet is off-centered, the reflections array splits into two interlacing arrays.

In the y direction the behavior is similar, except that the decay length is doubled since the image lattice has a doubled lattice constant. Therefore, there are two competing effects: the exponential decay in space and the divergence of amplitude as $\tan(\pi\gamma/2)$ due to confinement. Similarly to the unconfined case, we obtain the crystal potential by superposition of single-droplet potentials, then equate drag and friction on a single droplet and derive its equation of motion.¹²⁾ The dispersion relations are:

$$\omega_x(k) = -4B \sum_{j=1}^{\infty} \sin(jka) \coth(\pi j\beta) \operatorname{csch}^2(\pi j\beta), \quad (4.2)$$

$$\omega_y(k) = B \sum_{j=1}^{\infty} \sin(jka) [3 + \cosh(2\pi j\beta)] \operatorname{csch}^3(\pi j\beta),$$

where $B \equiv (u_d^\infty/u_{oil}^\infty)(u_{oil}^\infty - u_d^\infty)(\pi^2 R/W^2) \tan(\pi\gamma/2)$ and $\beta \equiv a/W$. Consistent with the experiment, the theory shows the x - y anti-symmetry breaking $|\omega_x(k)| < |\omega_y(k)|$ for all $k < \pi/a$ and fits the data satisfyingly without any adjustable parameters. The model predicts that C_s and ω diverge as $\gamma \rightarrow 1$. In this limit the droplets block the channel (plug flow), where it is difficult to pass liquid through the narrow necks, rendering the crystal effectively incompressible. These ‘harder’ modes are expected to have reduced amplitudes, as observed experimentally (Fig. 5(d)). The interplay between exponential decay and divergence of amplitude, leads to a non-monotonous behavior of C_s , which is different for the longitudinal and transversal modes.

§5. Conclusion and outlook

We studied the collective modes of a 1D crystal of droplets flowing in a 2D microfluidic channel. The symmetry-breaking flow field drives the system far from thermal equilibrium and induces long-range hydrodynamic interactions at very low Reynolds number. As a result, unique dispersion relations of acoustic modes emerge, reflecting the broken symmetry and interactions. Additionally, we showed that the sidewall boundaries screening of the long-range interactions. At the crossover between unconfined 2D flow and effective 1D flow, the spectra and speed of sound are non-monotonous, as a result of an interplay between screening and incompressibility. It would be interesting to extend the collective mode approach from 1D crystals to 2D systems, which may lead to unexplored spectra.

References

- 1) T. Thorsen, R. W. Roberts, F. H. Arnold and S. R. Quake, *Phys. Rev. Lett.* **86** (2001), 4163.
- 2) R. Dreyfus, P. Tabeling and H. Willaime, *Phys. Rev. Lett.* **90** (2003), 144505.
- 3) J. D. Tice, H. Song, A. D. Lyon and R. F. Ismagilov, *Langmuir* **19** (2003), 9127.
- 4) D. R. Link, S. L. Anna, D. A. Weitz and H. A. Stone, *Phys. Rev. Lett.* **92** (2004), 054503.
- 5) W. Engl, M. Roche, A. Colin, P. Panizza and A. Ajdari, *Phys. Rev. Lett.* **95** (2005), 208304.
- 6) P. Garstecki, M. J. Fuerstman and G. M. Whitesides, *Nature Physics* **1** (2005), 168.
- 7) P. Garstecki, M. J. Fuerstman and G. M. Whitesides, *Phys. Rev. Lett.* **94** (2005), 234502.
- 8) A. S. Utada, E. Lorenceau, D. R. Link, P. D. Kaplan, H. A. Stone and D. A. Weitz, *Science*, **308** (2005), 537.
- 9) P. Garstecki and G. M. Whitesides, *Phys. Rev. Lett.* **97** (2006), 024503.
- 10) H. Willaime, V. Barbier, L. Kloul, S. Maine and P. Tabeling, *Phys. Rev. Lett.* **96** (2006), 054501.
- 11) T. Beatus, T. Tlusty and R. Bar-Ziv, *Nature Physics* **2** (2006), 743.
- 12) T. Beatus, R. Bar-Ziv and T. Tlusty, *Phys. Rev. Lett.* **99** (2007), 124502.
- 13) H. M. Thomas and G. E. Morfill, *Nature* **379** (1996), 806.
- 14) B. Liu and J. Goree, *Phys. Rev. E* **71** (2005), 046410.
- 15) R. Lahiri and S. Ramaswamy, *Phys. Rev. Lett.* **79** (1997), 1150.
- 16) R. A. Simha and S. Ramaswamy, *Phys. Rev. Lett.* **83** (1999), 3285.
- 17) S. Ramaswamy, *Adv. Phys.* **50** (2001), 297.
- 18) M. Baron and J. Bławdziewicz and E. Wajnryb, *Phys. Rev. Lett.* **100** (2008), 174502.
- 19) S. Ramaswamy, J. Toner and J. Prost, *Phys. Rev. Lett.* **84** (2000), 3494.
- 20) R. Bar-Ziv, T. Tlusty and A. Libchaber, *Proc. Natl. Acad. Sci.* **99** (2002), 11589.
- 21) T. Tlusty, R. Bar-Ziv and A. Libchaber, *Phys. Rev. Lett.* **93** (2004), 258103.
- 22) H. Lamb, *Hydrodynamics* (Cambridge University Press, Cambridge, UK, 1993).
- 23) R. P. Feynman, R. B. Leighton and M. Sands, *The Feynman Lectures on Physics*, Vol. 2 (Addison-Wesley, Reading, MA, 1963), 7-5.